Biomimetic Architectures for the Impedimetric Discrimination of Influenza Virus Phenotypes

Bernd Wicklein[1], Mª Ángeles Martín del Burgo[2], María Yuste[2], Ester Carregal-Romero[3], Andreu Llobera[3], Margarita Darder[1], Pilar Aranda[1], Juan Ortín[4], Gustavo del Real[2], César Fernández-Sánchez[3,], and Eduardo Ruiz-Hitzky[1,]**

[*] Prof. E. Ruiz-Hitzky, eduardo@icmm.csic.es; Dr. C. Fernández-Sánchez, cesar.fernandez@imb-cnm.csic.es

1 Instituto de Ciencia de Materiales de Madrid, CSIC, C/ Sor Juana Inés de la Cruz 3 28049 Madrid, Spain

2 Instituto Nacional de Investigación y Tecnología Agraria y Alimentaria, Ctra. de la Coruña Km 7,5 28040 Madrid, Spain

3 Centro Nacional de Microelectrónica - IMB, CSIC, Campus UAB 08193 Cerdanyola del Vallès, Barcelona, Spain

4 Centro Nacional de Biotecnología, CSIC, Darwin 3, Campus de Cantoblanco, 28049 Madrid, Spain

Keywords: hybrid bilayers, biomimetic receptors, sialic acid, influenza A virus, phenotype discrimination, impedimetric detector

Abstract:

Rapid discrimination of avian *vs.* human phenotypes of emerging influenza A virus isolates with pandemic potential is an important issue in pathogenesis and epidemiology studies of the infection. In this work, we have tailored functional architectures on the surface of a gold electrode introducing receptor molecules as sensing entity that mimic those found in the membrane of target cells of the influenza A virus and with the aim of developing an impedimetric-based detector for influenza A virus phenotyping. In a bottom-up approach, the artificial receptors are built by sequential assembly of a 1-

octanethiol/octyl-galactoside hybrid bilayer, followed by an enzyme-mediated functionalization of the terminal galactoside groups with sialic acid molecules. The detection mechanism relies hence on the specific affinity between the sialic acid-galactose receptor moieties anchored on the modified electrode surface and the hemagglutinin (HA) viral surface protein. By using the appropriate type of sialyltransferase enzyme, sialylation of galactose residues is made through α-2,3 or α-2,6 linkages. This permits the envisaged impedimetric detector to discriminate rapidly between avian *vs.* human strains of influenza A virus with the absence of elaborate sample preparation steps. In contrast to immunosensors based on antibodies as bioreceptor, the sialylated modified gold electrode is also able to distinguish among influenza phenotypes, which could make the here presented detector a reagentless, label-free diagnostic device for influenza phenotyping.

1. Introduction

Pandemics occur when re-assorted influenza viruses, harboring avian surface glycoproteins, infect and spread among humans owing to a limited immunity against those new variants.[1],[2] To cross species barrier from birds to humans, pandemic influenza viruses require adaptation to human cells through acquisition of critical mutations mainly in the receptor binding protein, hemagglutinin (HA).[3] Permissive cells have at their surface influenza virus receptors consisting of sialic acid (SA) moieties linked to galactose terminals of glycoproteins, to which the hemagglutinin viral protein binds as the first step of virus infection[4],[5] (**Scheme 1**). The type of linkage between SA and the galactose groups determines the host specificity of influenza viruses, being the α-2,3 linkage specific for avian-like and the α-2,6 for human-like viruses.[6],[7]. This specificity correlates with the type of SA-galactose linkage expressed on host tissues, predominating the α-2,6 in human trachea and the α-

2,3 in the avian intestinal epithelium.[8] Genetic and phenotypic characterization of novel re-assorted viruses with pandemic potential is of utmost importance for rapid implementation of control measures and to understand the molecular mechanisms underlying inter-specific transmission of influenza viruses. Therefore, discrimination of pathogenic phenotypes of emerging influenza virus isolates is an important issue in epidemiology studies and surveillance of pandemics. Recurrent outbreaks of avian influenza and its transmission to humans have emphasized the need of efficient and reliable discrimination of receptor-binding, highly pathogenic viruses such as the H5N1, from other human influenza viruses.[9]

Existing standard diagnostic methods such as hemagglutination, ELISA, virus isolation cultures, RT-PCR, or gene sequencing are generally time-consuming, expensive, and may lack either sensitivity or specificity.[10],[11] These short-comings can be remedied by biosensors[12] and especially by those based on electrochemical detection methods which are typically rapid, sensitive, selective, and user-friendly.[13] Various impedimetric immunosensors for influenza virus detection have been presented that relied on the use of specific antibodies as bioreceptors for the virus target analyte.[12],[14],[15] However, the antibody performance is easily compromised by protein degradation when being immobilized on the transducer surface and by limited storage stability. Therefore, we followed a novel strategy based on the tailoring of receptors similar to those found in target cells as selective recognition elements of a biosensor. This approach comes from inspiration by naturally occurring structures like biological cell membranes. They are the host of a great variety of molecules acting as receptors in the interaction with the external environment [16] and are therewith of special interest for the development of novel biotechnological tools.[17],[18] In this context, this work reports the development of a selective, impedimetric sensor comprised of a miniaturized three-

gold electrode transducer configuration and a nanostructured biomimetic membrane inspired by the influenza virus receptor (Scheme 1).

A versatile route to achieve such biomimetic membranes on the surface of a gold transducer can be provided by the concept of supported hybrid bilayers as an interesting development of the bilayer lipid membrane.[19],[20] The two halves of the membrane may consist of different (bio)surfactants that are held together by hydrophobic interaction of the hydrocarbon chains facing each other. This chemical approach can offer enhanced versatility in the design of functional interfaces and mimetism of biological surfaces. Illustrative examples are genetic biochips[21] or hybrid red blood cell membranes.[22] Typically, the anchoring bottom leaflet consists of alkane thiols or silanes, which strongly adhere on metal or silica/silicate surfaces, respectively, thereby giving rise to self-assembled monolayers (SAMs) and turning the modified surfaces hydrophobic. The upper leaflet can be constituted of biosurfactants that introduce specific functionalities to the surface. Especially those of natural origin such as lipids, glycolipids, lipopolysaccharides, lipopeptides, or sugar-based surfactants are frequently used.[23],[24],[25] Among the different surface analytical techniques used for studying layer deposition processes electrochemical impedance spectroscopy is a powerful tool that has been applied to probe and characterize the molecular structure of thin, organic surface layers, ranging from mixed thiol SAMs,[26] Langmuir-Blodgett derived lipid cell mimics,[27] and to monitor surface adhered cell phenomena, which could be applied as a transduction mode for biosensing.[28], [29], [30]

Here, we present the combination of different chemistries related to bilayer formation and enzyme-mediated sialylation of galactose terminals, for the formation of nanostructured hybrid bilayers on gold electrodes that mimic the viral receptors of target cells. This nanostructure involves the self-assembling of 1-octanethiol and octyl-

galactoside layers, the latter being further functionalized with sialic acid groups by using the appropriate type of sialyltransferase enzyme. This simple protocol leads to a novel type of impedance-based biosensor device incorporating biomimetic sialic acid-galactose receptors that allows the fast discrimination of phenotypes of influenza virus isolates.

2. Results and Discussion

The influenza biosensor was prepared in a bottom-up approach by stepwise deposition of individual SAMs. Octyl-galactoside (OGal) containing hybrid biofilms were prepared on gold electrode surfaces using 1-octanethiol (Othiol) as the surface modifying component, which is well known to form densely-packed SAMs on gold.[31] The assembly of OGal to form the upper leaflet took place by adsorption onto the formed Othiol SAM, and eventually gave rise to a hybrid Othiol-OGal bilayer. The surface analytical techniques used in this work for substantiating our layer build-up examinations were electrochemical impedance spectroscopy (EIS), cyclic voltammetry (CV), x-ray photoelectron spectroscopy (XPS), water contact angle measurements, and atomic force microscopy (AFM). **Figure 1** shows the impedance spectra in the form of Nyquist plots of the gold electrochemical cell recorded after each modification step. These impedance data were analyzed by fitting the recorded spectra to a simple Randles equivalent circuit model (Figure 1b), which simply describes the electrical behavior of an electrochemical cell in contact with a liquid solution.[32] This model includes discrete electrical components and renders values for the electrical double layer capacitance introducing a constant phase element (CPE_{dl}), for the charge transfer resistance R_{ct}, for the impedance related to interfacial mass diffusion (the so-called Warburg impedance, W), and for the solution resistance R_S. The CPE_{dl}, R_{ct} and W are closely related to

interfacial properties such as surface layer density, layer imperfections, or surface roughness [33], [34] and so EIS has become an established technique to characterize surface confined membranes.[27], [35], [36] As will be shown below, the high sensitivity of EIS to the detection of interfacial phenomena was not only used in this work as a characterization technique to probe the layer architecture of the virus biosensor, but also as the transduction mode of the resulting biosensor for the detection of the viral particles.

On bare Au, a small semi-circle characteristic of the CPE_{dl} and the R_{ct} generated at the liquid-surface interface is recorded. The layer formation increases stepwise the radii of the semi-circles, this being related to an increase of the R_{ct} and a decrease of the CPE_{dl} at the modified electrode surface. Generally, high R_{ct} values are indicative of densely packed surface layers that hamper the charge transfer of the redox probe at the solution/electrode interface.[37] This is also reflected in the recorded cyclic voltammograms after each modification step, where the capacitive currents steadily decreased (see **Figure S2**).

Similar information can be extracted from the characterization data recorded for the optimization of the bilayer formation conditions. In these studies (**Figure 2**), it has been found that both adsorption time and concentration of OGal in the incubation solution are critical for the formation of a compact Othiol-OGal bilayer. Advancing water contact angle measurements were performed to investigate the change of surface hydrophobicity during the subsequent layer depositions (Figure 2a). The contact angle on Au increased from 85º to 106º after formation of the Othiol SAM, which is comparable to reported data.[31] After one day incubation in 5 mM OGal solution, the contact angle decreased only marginally but a three-day incubation time resulted in a substantial decay to 81º. Waltermo and coworkers measured a water contact angle of

85º after octyl-glucoside adsorption (from 5 mM) on hydrophobized mica,[38] which is a value in good agreement with the data obtained in the present work. The drop in surface hydrophobicity is assumed to be related to an increased amount of galactoside headgroups at the solid/liquid interface that renders the surface more hydrophilic.

The dependence of the OGal adsorption on the incubation time was investigated by impedance measurements. Thiolated gold electrodes were immersed in 5 mM OGal solution for 1, 2, and 5 days and the corresponding R_{ct} values are reported in **Table 1**. It is apparent that the relative R_{ct} decreased with extended OGal incubation times even though the absolute R_{ct}(OGal) was always above R_{ct}(Othiol). This is indicative for reduced compactness of the formed Othiol-OGal bilayer upon prolonged incubation. In order to clarify whether Othiol molecules were apparently being replaced by OGal or simply removed without substitution, voltammetric thiol desorption experiments were performed (**Figure S3**). The results demonstrate a decrease in Othiol surface coverage with increased immersion time (Figure 2b). This observation suggests a damage of the initially formed 1-octanethiol SAM upon prolonged incubation. The fact that the absolute R_{ct}(OGal) value is still higher than R_{ct}(Othiol) could indicate that the removed Othiol molecules were partially replaced by OGal and thus, passivated the bare Au surface sites to some extent. This assumption is also consistent with the results from the water contact angle measurements, which suggest elevated OGal presence at the surface after three days despite of the Othiol SAM damage. As for a hypothesis, it is also known that short chain alkanethiols ($n < 10$) form more defective and less compact SAMs which consequently are more prone to desorption.[31] This may allow for the intercalation of OGal molecules into the Othiol SAM that could reach the gold surface where they eventually may replace Othiol molecules. This assumption was also

supported by experiments where the SAM was formed with 1-dodecylthiol that gave rise to more compact layers. It has been noticed that the amount of adsorbed OGal molecules was significantly lower than the amount adsorbed on a 1-octanethiol SAM (data not shown). Therefore, these findings can be interpreted that OGal interpenetration was impeded on the 1-dodecylthiol SAM while the higher OGal content on the 1-octanethiol SAM should be due then to intercalation.

The next parameter under investigation is the OGal concentration of the incubation solution. Octanethiolated Au electrodes were immersed in various OGal solutions (0.5-5 mM) for one day. The EIS results show a slight rise in the relative R_{ct} for increased OGal concentration (Figure 2c), but this increase is not significant, which suggests that the OGal concentration might not be the key to generate a compact upper leaflet of the Othiol-OGal bilayer.

In conclusion, the optimized conditions used for the subsequent sialylation were chosen to be one day incubation in 5 mM OGal since under these conditions a high amount of galactose groups were incorporated on the electrode surface and the Othiol SAM distortion appeared not to be highly affected.

Atomic force microscopy was employed to study the formation of the multilayer structure and to examine the compositional homogeneity of the Othiol-OGal bilayer. For this purpose, topographic images with the corresponding surface roughness values (RMS) were collected together with a frequency shift image which can reveal variations in the chemical composition of the studied surface (**Figure 3**). The bare, polycrystalline gold surface has a RMS value of 2.6 nm. Upon formation of the Othiol SAM the RMS increases to 3.0 nm. After the subsequent deposition of the outer OGal leaflet and SA molecules the topographic images (Figure 3 c,d) show the disappearance of the crystalline grain structure and reveal a further rise in RMS to 3.5 and 3.8 nm,

respectively. This tendency demonstrates the successive deposition of the organic layers. In addition, the domains of different contrast in the frequency image in Figure 3 e indicate certain compositional heterogeneity of the bilayer. The AFM study confirms therewith the already assumed defects upon bilayer formation that the electrochemical characterization appeared to show.

The resultant Othiol-OGal biofilm was then modified with SA molecules in order to be applied as the recognition element of an affinity biosensor for the phenotypes of the influenza virus. The specificity of the conceived sensor lies in the affinity of specifically linked sialic acid-galactoside moieties for the hemagglutinin of avian *vs*. human influenza viruses. The incorporation of these SA molecules in the Othiol-OGal biofilm occurs via sialylation of galactoside residues with the corresponding α-2,6 or α-2,3-(N)-sialyltransferase (SAT) enzyme.

XPS was employed to verify the presence of linked sialic acid molecules by examining the photoelectron bands of C1s, O1s and N1s. **Figure 4a** shows XPS core level spectra of an α-2,6 SA terminal surface together with the underlying Othiol and OGal layers for comparison. Deconvolution of the C1s band revealed components at 288.9 eV, 287.2 eV, and 285.7 eV, which can be attributed to COO^-, C=O, and C-N functions,[39] respectively, which are only present in the sialic acid molecule. The underlying OGal and Othiol molecules contribute with bands at 286.5 eV (C-O-C), at 284.6 eV (C-(C,H)), and at 285.8 eV (C-S), respectively. The N1s band at 400.5 eV revealed the presence of unprotonated amine groups,[39] attributable to the neuraminic acid moiety of the sialic acid molecule. Nitrogen was not detected in the underlying Othiol-OGal bilayer, confirming SA as the only source of the observed N1s band. The deconvolution of the O1s peak reveals a band at 531.2 eV, which is attributed to

carboxylic acid functions (O=C)[39] and is therefore associated with the presence of the sialic acid moieties. Furthermore, the O1s peak from the OGal terminated surface is decomposed into a band at 533.4 eV (H_2O molecules) and at 531.8 eV that can be associated to hydroxyl (C-OH) and acetal (C-O-C) functions of the galactose ring.[39] Altogether, the results confirm the presence of the expected molecules and that the OGal layer is successfully sialylated with the α-2,6 linkage.

Additionally, XPS spectra of Au-Othiol and Au-Othiol-OGal samples were recorded to evaluate possible damage of the layers from ambient oxidation of the bottom Othiol SAM. Figure 4a shows the signal of S2p at a binding energy close to 162 eV. In both cases, the splitting between the S2p1/2 and S2p3/2 photoelectron lines was observed, being 0.94 eV for the Au-Othiol sample and 1.10 eV for the Au-Othiol-OGal sample. It is also evident from both spectra the absence of signals at 163 eV that would indicate the presence of –SH groups due to inspecifically adsorbed molecules.

The band centered at 168 eV is attributed to the slight oxidation of the thiol group.[40],[41] Taking into account the areas of the different signals, the Au-Othiol sample shows a content of 13.3% oxidized sulfur and 86.7% thiolated sulfur, while in the Au-Othiol-OGal sample the amount of oxidized sulfur is close to 8.6%. In both cases, the extent of the oxidation is small enough and we can assume that the hybrid bilayer maintains its integrity, as already observed in analogous systems.[40]

The success of the sialylation process as well as the ability of the resulting sialic acid-galactose system to act as viral receptor can also be confirmed by means of a Western Blot (WB) assay. For instance, the sialylation using an α-2,3 SAT was tested by incubating the resulting modified surfaces with a H5N9 influenza virus strain (A/turkey/Wisconsin/1/1968). This is an avian influenza virus whose HA binds specifically to α-2,3 linked sialic acid groups. The adsorbed viral particles can then be

revealed by a WB assay. The results clearly reveal typical stains on the sialylated surfaces which confirms the presence of adsorbed H5N9 virus particles and therewith, the specific functionalization with α-2,3 bonded SA groups (Figure 4b). Overall, the characterization studies of the modified electrode surfaces demonstrate the presence of attached SA moieties and therewith, resemble the surface of virus target cells (Scheme 1).

The response of the developed biosensor is based on EIS measurements,[13] which, as mentioned above for the characterization studies, can be highly sensitive to slight changes at the double layer due, in this case, to the interaction of the virus with the modified sensor surface. Non-sialylated gold electrodes just modified with the Othiol-OGal bilayer show only a slight increase in R/R_{blank} possibly due to a weak unspecific virus adsorption (**Figure 5a**). In contrast, α-2,6 sialylated electrodes clearly demonstrate significantly increased R/R_{blank} values attributed to the specific interaction with the human influenza virus strain H1N1 (A/PR/8/34), as shown in Figure 5a. Additional support is also provided from WB images of sialylated gold chips (inset in Figure 5a) that confirm the specific attachment of H1N1 virus particles on the α-2,6 SA modified surface by the appearance of dark stains whereas in the absence of SA no stains can be observed.

The developed biosensor was further tested at low virus concentrations (0.05, 0.075, and 0.1 μg ml^{-1}), in order to roughly estimate its sensitivity. Figure 5b shows that R/R_{blank} steadily increased over the total incubation time for the three assayed concentrations. For a fixed incubation time (45 min) the signal follows a linear relationship with the virus concentration and a sensitivity value of 20.1 $(\mu g/ml)^{-1}$ could be estimated (inset in Figure 4b). Furthermore, the response of the biosensor is very fast

and clear differences could be recorded after a 6 min incubation time, as observed in kinetic experiments (see **Figure S4**). This very short response time furnishes the present biosensor with a great advantage over many standard clinical methods such as real-time polymerase chain reaction (RT-PCR), antigen tests, immunofluorescence, ELISA, or viral culture,[10],[11] which are in some cases subjected to long revelation periods over several hours or even days. **Figure S5** depicts the response with time of two individual sensors and points out the nice reproducibility of the sensor to the detection of H1N1 virus.

AFM imaging of electrode surfaces after virus detection indicated individually adsorbed viral particles (Figure 5c) in a comparable fashion to observations made by Wang et al.[14] of adsorbed H5N1 virions on the electrode surface of an immunosensor. The specific SA sites on the electrode surface may account for this behavior and in turn give rise to the low detection limit of the here presented biosensor approach. The theoretical detection limit was estimated to be 0.024 μg ml^{-1} (interception point of trend curve with y=1 in Figure 5b). This is by two orders of magnitude lower than other reported impedimetric influenza biosensors based on whole virion detection without special sample pre-treatment.[15],[14] In other cases, such as impedimetric genosensors,[42] the genetic material of influenza viruses is used for detection,[43] which implies extraction of DNA or RNA, and in some cases even their amplification by the PCR method. This requires elaborate sample preparation and biotechnological training of the user, making the whole process tedious and not user-friendly. The detection limit reached in the present work would be low enough for practical phenotyping assays with enriched virus samples.

Efficient transmission of avian strains to humans and further person-to-person propagation is mostly determined by the ability of the HA protein of the avian virus to

recognize specific SA receptors on the human cells. In the recent years, there have been a number of cases of transmission of avian virus to humans including those of the highly pathogenic H5N1 strain which so far are responsible of more than 340 deaths in 15 different countries.[9] Rapid discrimination of receptor-binding phenotypes of emerging influenza virus isolates is thus an important issue in pathogenesis and epidemiology studies of the infection. Therefore, a biosensor being able to discriminate between avian (α-2,3-specific) and human (α-2,6-specific) influenza isolates would be a very useful tool to detect the presence of the avian isolates with pandemic potential. It would be also useful for measuring the degree of adaptation of avian influenza viruses to human hosts in terms of receptor affinity as well as research tool for the assessment of critical amino acid residues in modified HA involved in receptor binding and host-specificity.[44] The selectivity of the α-2,6 sialylated biosensor is shown in **Figure 6**. A R/R_{blank} value of 2.6 was obtained for a human H1N1 influenza virus whereas no signal above the blank was obtained for an avian H5N9 virus. The α-2,3 sialylated biosensor exhibited a significant selectivity toward the corresponding H5N9 virus (R/R_{blank}= 1.9). Human H1N1 (PR8) virus, despite of exhibiting preferential affinity for the α-2,6 receptor, is also detected by this biosensor although at lower extent (R/R_{blank} = 1.4). Such dual recognition was also observed in conventional hemagglutination assays using de-asylated/α-2,3 or 2,6-re-asylated chicken erythrocytes (**Table S1**), which supports the recorded biosensor response by revealing the fact that some strains can exhibit affinity to both types of receptor.[45] This fact has been previously demonstrated to originate from avian-adaption of egg-incubated influenza strains, developing a shift in the receptor-binding phenotype toward interaction with α-2,3 sialic acid receptors.[46] This example underlines the usefulness of the here developed biosensor for qualitative evaluation of phenotype shifts.

Overall, the here presented results confirm the conceived concept of selectivity afforded by the choice of the corresponding sialyltransferase enzyme and even point toward the possibility to assess the degree of HA adaptation to human or avian target cells in terms of relative affinity to one or another biosensor.

To test the specificity of the present biosensor, we used the PRRS virus that commonly accompanies influenza viruses in the porcine respiratory complex and is frequently present in respiratory clinical samples as nasal exudates. PRRS viruses are, like influenza, enveloped viruses but lack the specific proteins that bind sialic-bearing surface molecules.[47] Figure 5d displays the sensor response for the PRRS virus together with that recorded in serum (background). As can be noticed, the test with PRRS virus did not give a signal above the background and the biosensor can therefore be considered to be non-specific for this virus. The present results imply that the adsorption mechanism is essentially based on the specific interactions between the viral hemagglutinin and the sialic acid sites. A further control was conducted with non-inactivated H1N1 virus to rule out potential alterations of the virus membrane structure inflicted by the UV treatment and that could consequently affect the correct detection. The R/R_{blank} curve of active H1N1 in Figure 4d shows a steady increase with incubation time. The R/R_{blank} value at 45 min is 1.9 which is comparable to the one recorded with a 0.075 $\mu g\ ml^{-1}$ concentration of inactivated H1N1 virus. Given the low concentration of 0.01 $\mu g\ ml^{-1}$ of the active virus applied, this signal substantiates a very high sensitivity of the sensor for active viruses. Considering these observations, it can be suggested that the inactivated H1N1 virus might have suffered from protein damage, which reduced its detectability by the present biosensor setup based on ligand-receptor affinity.

3. Conclusions

In summary, we have successfully transferred a receptor concept originating from the membrane of target cells to the surface of a sensing device. A hybrid Othiol-OGal membrane was prepared for that purpose by sequential adsorption of the two membrane leaflets. The optimized conditions were found to be incubation of the Othiol SAM for one day in 5 mM OGal. The sialylation of these bilayers with the specific SAT enzymes could provide α-2,3 and α-2,6 linked SA groups. This allowed for the preparation of biosensors selective to influenza virus receptor-phenotypes, based on the affinity between the specific sialic acid groups and the viral hemagglutinin. The resultant affinity biosensor could successfully detect and distinguish between human (H1N1) and avian (H5N9) isolates. The impedimetric sensing approach shows short response times and high sensitivity. A further advantage of the present biosensor is that no sample preparation is required. Thus, the influenza biosensor conceived and prepared in this work is "easy to handle", fast, cheap and could be very convenient for phenotype characterization of viral isolates. Additionally, the versatility of this layer-by-layer approach permits a possible expansion toward the detection of other human and veterinarian viruses by incorporation of the corresponding cellular receptor molecules on the detector surface.

4. Experimental

Materials: All chemicals and biological material were purchased from Sigma-Aldrich unless otherwise noted.

Biosensor preparation: An on-chip three-electrode electrochemical cell was used for the fabrication of the Influenza virus biosensor. The chip layout and its fabrication

details are provided in **SI**. The bare gold electrodes were initially cleaned with ethanol, rinsed in water and dried under a N_2 stream. Then, an electrochemical activation step was carried out in a KNO_3 solution (0.1 M) by cycling the potential between +0.2 V and -2.2 V (vs. Ag/AgCl reference electrode), 40 times at a 100 mV s^{-1} scan rate. This treatment gave rise to a clean gold electrode surface, which was tested in a KNO_3 solution (0.5 M) containing a ferrocyanide/ferricyanide redox pair (2 mM). The cleaned electrodes were immersed overnight (ca. 16 h) in 1-octanethiol (Otiol) solution (1 mM) in ethanol. The surfaces were rinsed with copious ethanol and then dipped in an aqueous octyl-galactoside (OGal, from Carbosynth, UK) solution at different concentrations and varying incubation times. The adsorption was carried out by means of an α-2,6-sialyltransferase enzyme (SAT) from *Photobacterium damsela* (EC 2.4.99.1) and α-2,3-SAT from *Pasteurella multocida* (EC 2.4.99.4). For instance, 18 µl of α-2,6-SAT stock solution (160 µg/ml) were mixed with 180 µl of the substrate cytidine-5'-monophospho-N-acetylneuraminic acid sodium salt (CMP-sialic acid) (at 5 mg ml^{-1}) and 1080 µl PBS. The as-modified gold surfaces were kept in this solution for 4 h at 37 ºC, subsequently rinsed with phosphate buffer saline (PBS) and placed overnight in bovine serum albumin (BSA) solution (2 %) to block any unspecific adsorption sites. Until use, the sialylated electrodes were stored in PBS at 4 ºC. 0.8×0.8 cm^2 gold chips, prepared by evaporation of Cr and Au on 4-inch Si/SiO_2 substrates as described above, were employed for comparative Influenza virus detection using Western Blot assays.

Biofilm characterization: XPS spectra were recorded on a VG Escalab 200 R using monochromatic Al Kα radiation at 1486.7 eV (200 W, 12 kV) in the non-focusing mode under UHV. The photoelectron energy was analyzed with a PHOIBOS 150 9MCD and a multi-channeltron detector. The binding energies for each spectrum were calibrated

with respect to the C1s band at 284.6 eV. AFM images were acquired in dynamic mode on a Nanotec AFM instrument equipped with a Si cantilever. The force constant of the cantilever was 2.8 N m^{-1} and the resonance frequency 75 kHz. Dynamic water contact angle measurements were performed on a Krüss drop shape analysis system (Germany). Western Blot images, using a M58-Biotin/Streptavid-HRP combination for virus detection, were obtained on a ChemiDoc™ XRS+ system from Bio-Rad (CA, USA).

Electrochemical analysis: Electrochemical impedance spectroscopy (EIS) measurements were performed on a Frequency Response Analyzer SI 1255 HF from Schlumberger connected to the Solartron 1480 MultiStat potentiostat, in the measurement electrolyte composed of PBS (6.7 mM, pH 7.3) containing KNO_3 (0.5 M) and $Fe(CN)_6^{4-/3-}$ (2 mM) as redox pair. The frequency range, modulation amplitude and DC potential were set to 100 kHz -1 Hz (10 data points per decade), 10 mV, and -8 mV (this potential corresponding to the half-wave potential of the Fe^{3+}/Fe^{2+}redox pair *vs*. Au pseudo-ref. potential), respectively. The Nyquist plots of the EIS spectra were fitted to a Randles equivalent circuit model.[32] Othiol surface coverage was estimated by integration over the cathodic peaks in voltammograms obtained from Othiol desorption experiments as detailed in SI.

Influenza virus detection using EIS: Virus detection was carried out by EIS with the modified gold electrodes as described above. The as-prepared biosensors were firstly subjected to an EIS measurement in order to record the blank values. Subsequently, the electrodes were incubated with virus containing aliquots prepared from a purified PR8/34 (H1N1) virus stock solution (800 μg ml^{-1}). This H1N1 stock was inactivated by exposure to UV light prior to the assays. Working solutions of different H1N1

concentrations were prepared on a daily basis and always kept at 4 ºC. Drops of 50 μl were placed on the electrode and kept under humid atmosphere to prevent solvent evaporation. After 15 min the electrode was rinsed with PBS and dipped in the measurement electrolyte for EIS. Control measurements were conducted with the PRRS (Porcine Respiratory and Reproductive Syndrome) virus and the H5N9 influenza virus strain (A/turkey/Wisconsin/1/1968), which were suspended in PBS containing mouse serum and BSA. For the selectivity test study (EIS measurements) the H1N1 virus sample was suspended in BSA/PBS (0.5%) solution at a virus concentration of 0.1 μg ml^{-1}. The corresponding blank recordings were performed with BSA/PBS solution (0.5 %). The H5N9 virus was present in serum at a stock concentration of 800 μg ml^{-1} and diluted with BSA/PBS (0.5 %) to 0.75 μg ml^{-1}. All virus concentrations are estimated on the basis of total viral protein concentration.

Acknowledgements

This work was supported by the CICYT (Spain, projects MAT2009-09960 and AGL2007-60274) and the CSIC (Spain, projects PIF08-018 and 201060I009). BW acknowledges a *personal investigador* contract of the Comunidad de Madrid. MAMB and MY acknowledge a PIF08-018 contract. Furthermore, we thank Prof. L. Vázquez and Prof. J.A. Martín Gago for the discussion of the AFM and XPS data.

Supporting Information. Figures S1 to S5 and Table S1. Supporting Information is available online from Wiley InterScience or from the author.

Received: ((will be filled in by the editorial staff))
Revised: ((will be filled in by the editorial staff))
Published online: ((will be filled in by the editorial staff))

References.

[1] C. Korteweg, J. Gu, *Am. J. Pathol.* **2008**, *172*, 1155.
[2] S. M. Zimmer, D. S. Burke, *N. Engl. J. Med.* **2009**, *361*, 279.
[3] S. Chutinimitkul, S. Herfst, J. Steel, A. C. Lowen, J. Ye, D. van Riel, E. J. A. Schrauwen, T. M. Bestebroer, B. Koel, D. F. Burke, K. H. Sutherland-Cash, C. S. Whittleston, C. A. Russell, D. J. Wales, D. J. Smith, M. Jonges, A. Meijer, M. Koopmans, G. F. Rimmelzwaan, T. Kuiken, A. D. M. E. Osterhaus, A. García-Sastre, D. R. Perez, R. A. M. Fouchier, *J. Virol.* **2010**, *84*, 11802.
[4] C. Traving, R. Schauer, *Cell. Mol. Life Sci.* **1998**, *54*, 1330.
[5] R. Schauer, *Glycoconj. J.* **2000**, *17*, 485.
[6] D. C. Wiley, J. J. Skehel, *Ann. Rev. Biochem.* **1987**, *56*, 365.
[7] I. Stephenson, J. M. Wood, K. G. Nicholson, M. C. Zambon, *J. Med. Virol.* **2003**, *70*, 391.
[8] J. N. Couceiro, J. C. Paulson, L. C. Baum, *Virus Res.* **1993**, *29*, 155.
[9] D. Vijaykrishna, L. L. M. Poon, H. C. Zhu, S. K. Ma, O. T. W. Li, C. L. Cheung, G. J. D. Smith, J. S. M. Peiris, Y. Guan, *Science* **2010**, *328*, 1529.
[10] Centers for Disease Control and Prevention, Interim Guidance on Specimen Collection, Processing, and Testing for Patients with Suspected Novel Influenza A (H1N1) Virus Infection. http://www.cdc.gov/h1n1flu/specimencollection.htm (accessed Nov. 2011).
[11] L. L. M. Poon, K. H. Chan, G. J. Smith, C. S. W. Leung, Y. Guan, K. Y. Yuen, J. S. M. Peiris, *Clin. Chem.* **2009**, *55*, 1555.
[12] R. L. Caygill, G. E. Blair, P. A. Millner, *Anal. Chim. Acta* **2010**, *681*, 8.
[13] J.-G. Guan, Y.-Q. Miao, Q.-J. Zhang, *J. Biosci. Bioeng.* **2004**, *97*, 219.
[14] R. Wang, Y. Wang, K. Lassiter, Y. Li, B. Hargis, S. Tung, L. Berghman, W. Bottje, *Talanta* **2009**, *79*, 159.
[15] M. F. Diouani, S. Helali, I. Hafaid, W. M. Hassen, M. A. Snoussi, A. Ghram, N. Jaffrezic-Renault, A. Abdelghani, *Mater. Sci. Eng.: C* **2008**, *28*, 580.
[16] G. van Meer, *Nat. Rev. Mol. Cell Biol.* **2008**, *9*, 112.
[17] B. Wicklein, M. Darder, P. Aranda, E. Ruiz-Hitzky, *Langmuir* **2010**, *26*, 5217.
[18] B. Wicklein, M. Darder, P. Aranda, E. Ruiz-Hitzky, *ACS Appl. Mater. Interfaces* **2011**, *3*, 4339.
[19] R. P. Richter, R. Bérat, A. R. Brisson, *Langmuir* **2006**, *22*, 3497.
[20] A. Mechler, S. Praporski, S. Piantavigna, S. M. Heaton, K. N. Hall, M. I. Aguilar, L. L. Martin, *Biomaterials* **2009**, *30*, 682.
[21] C. Xu, P. Taylor, M. Ersoz, P. D. I. Fletcher, V. N. Paunov, *J. Mater. Chem.* **2003**, *13*, 3044.
[22] J. B. Hubbard, V. Silin, A. L. Plant, *Biophys. Chem.* **1998**, *75*, 163.
[23] F. M. Menger, M. E. Chlebowski, A. L. Galloway, H. Lu, V. A. Seredyuk, J. L. Sorrells, H. L. Zhang, *Langmuir* **2005**, *21*, 10336.
[24] E. Gharaei-Fathabad, *Am. J. Drug Disc. Develop.* **2011**, *1*, 58.
[25] M. Deleu, M. Paquot, P. Jacques, P. Thonart, Y. Adriaensen, Y. F. Dufrene, *Biophys. J.* **1999**, *77*, 2304.
[26] Y. F. Xing, S. F. Y. Li, A. K. H. Lau, S. J. O'Shea, *J. Electroanal. Chem.* **2005**, *583*, 124.
[27] B. Lindholm-Sethson, *Langmuir* **1996**, *12*, 3305.
[28] A. Bouafsoun, S. Helali, S. Mebarek, C. Zeiller, A.-F. Prigent, A. Othmane, A. Kerkeni, N. Jaffrézic-Renault, L. Ponsonnet, *Bioelectrochemistry* **2007**, *70*, 401.

[29] R. de la Rica, A. Baldi, C. s. Fern„ndez-S„nchez, H. Matsui, *Anal. Chem.* **2009**, *81*, 3830.
[30] R. de la Rica, S. Thompson, A. Baldi, C. Fernandez-Sanchez, C. M. Drain, H. Matsui, *Anal. Chem.* **2009**, *81*, 10167.
[31] C. D. Bain, E. B. Troughton, Y. T. Tao, J. Evall, G. M. Whitesides, R. G. Nuzzo, *J. Am. Chem. Soc.* **1989**, *111*, 321.
[32] C. Fernandez-Sanchez, C. J. McNeil, K. Rawson, *Trends Anal. Chem.* **2005**, *24*, 37.
[33] R. K. Mendes, R. S. Freire, C. P. Fonseca, S. Neves, L. T. Kubota, *J. Braz. Chem. Soc.* **2004**, *15*, 849.
[34] S.-J. Ding, B.-W. Chang, C.-C. Wu, M.-F. Lai, H.-C. Chang, *Anal. Chim. Acta* **2005**, *554*, 43.
[35] G. Valincius, T. Meškauskas, F. Ivanauskas, *Langmuir* **2011**, *28*, 977.
[36] W. K. Chang, W. C. Wimley, P. C. Searson, K. Hristova, M. Merzlyakov, *Biochim. Biophys. Acta - Biomembranes* **2008**, *1778*, 2430.
[37] S. J. Ding, B. W. Chang, C. C. Wu, M. F. Lai, H. C. Chang, *Anal. Chim. Acta* **2005**, *554*, 43.
[38] Å. Waltermo, P. M. Claesson, I. Johansson, *J. Colloid Interface Sci.* **1996**, *183*, 506.
[39] P. A. Gerin, P. B. Dengis, P. G. Rouxhet, *J. Chim. Phys.* **1995**, *92*, 1043.
[40] M. H. Schoenfisch, J. E. Pemberton, *J. Am. Chem. Soc.* **1998**, *120*, 4502.
[41] C. Vericat, M. E. Vela, G. A. Benitez, J. A. M. Gago, X. Torrelles, R. C. Salvarezza, *J. Phys.: Condens. Matter* **2006**, *18*, R867.
[42] F. Lucarelli, G. Marrazza, A. P. F. Turner, M. Mascini, *Biosens. Bioelectron.* **2004**, *19*, 515.
[43] A. Bonanni, M. I. Pividori, M. Del Valle, *Analyst* **2010**, *135*, 1765.
[44] I. Ramos, D. Bernal-Rubio, N. Durham, A. Belicha-Villanueva, A. C. Lowen, J. Steel, A. Fernandez-Sesma, *J. Virol.* **2011**, *85*, 4421.
[45] L. Glaser, D. Zamarin, H. M. Acland, E. Spackman, P. Palese, A. Garcia-Sastre, D. Tewari, *Glycoconj. J.* **2006**, *23*, 93.
[46] A. S. Gambaryan, A. B. Tuzikov, V. E. Piskarev, S. S. Yamnikova, D. K. Lvov, J. S. Robertson, N. V. Bovin, M. N. Matrosovich, *Virology* **1997**, *232*, 345.
[47] K. D. Rossow, *Vet. Pathol. Online* **1998**, *35*, 1.

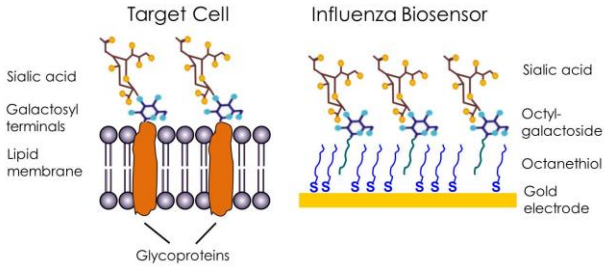

Scheme 1. Schematic representation of the membrane of an influenza virus-permissive cell and the structural comparison with the here presented influenza biosensor.

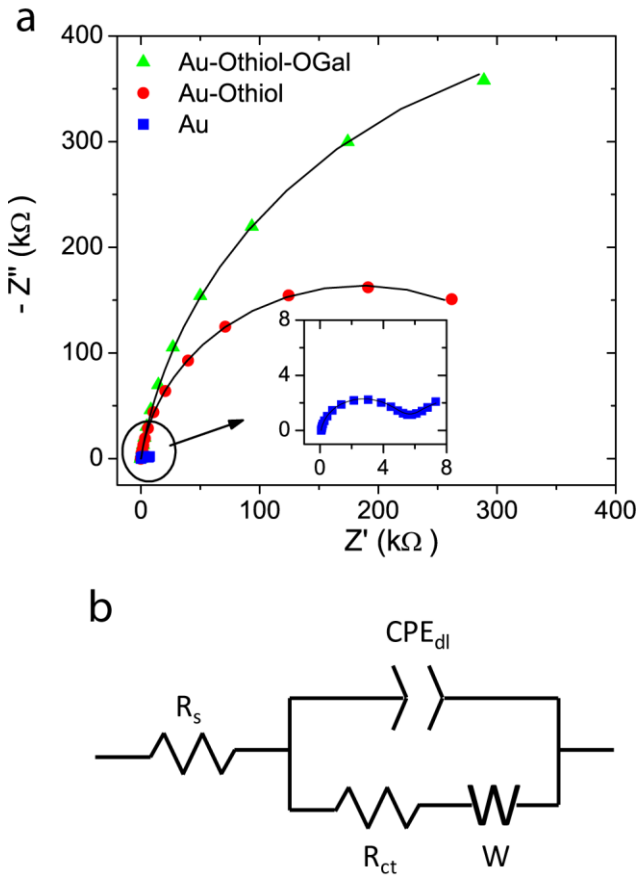

Figure 1. Impedance spectra in the form of Nyquist plots (Z' *vs.* Z") recorded with the bare Au surface and after being modified with the Othiol and OGal layers (a). The solid lines represent the fitting of data using the Randles equivalent circuit. The measurement electrolyte was composed of PBS (6.7 mM, pH 7.3) containing KNO_3 (0.5 M) and $Fe(CN)_6^{4-/3-}$ (2 mM) as redox pair. The frequency range, modulation amplitude, and DC potential were set to 100 kHz - 1 Hz, 10 mV, and -8 mV, respectively. Figure 1b displays the representation of a Randles equivalent circuit model used for analysis and interpretation of the EIS data.

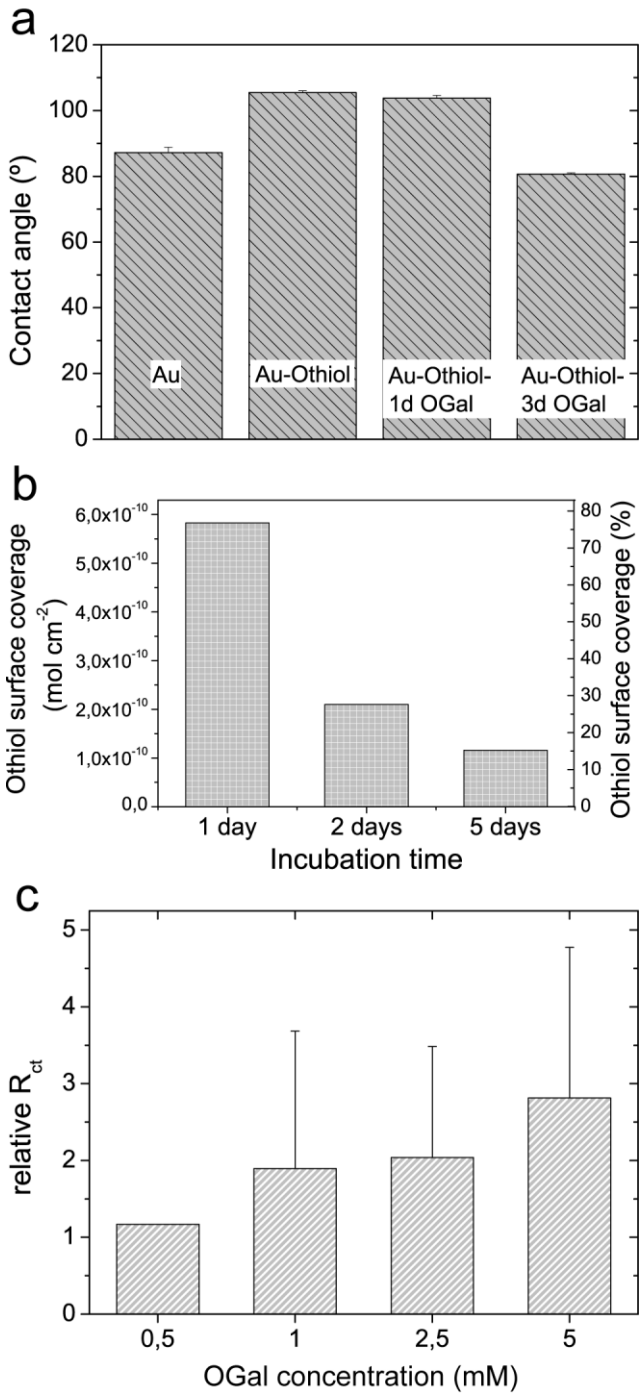

Figure 2. Advancing water contact angle measurements (a) on a bare Au surface and octanethiolated gold chips incubated in OGal (5 mM) for 1 and 3 days. (b) The surface coverage of Othiol on Au electrodes as function of the OGal incubation as deduced from voltammetric thiol desorption experiments in deareated NaOH solution (0.5 M). (c) The relative R_{ct} of Othiol-OGal modified gold electrodes as function of the OGal

concentration for one day incubation time. Error bars represent the standard deviation of at least two measurements.

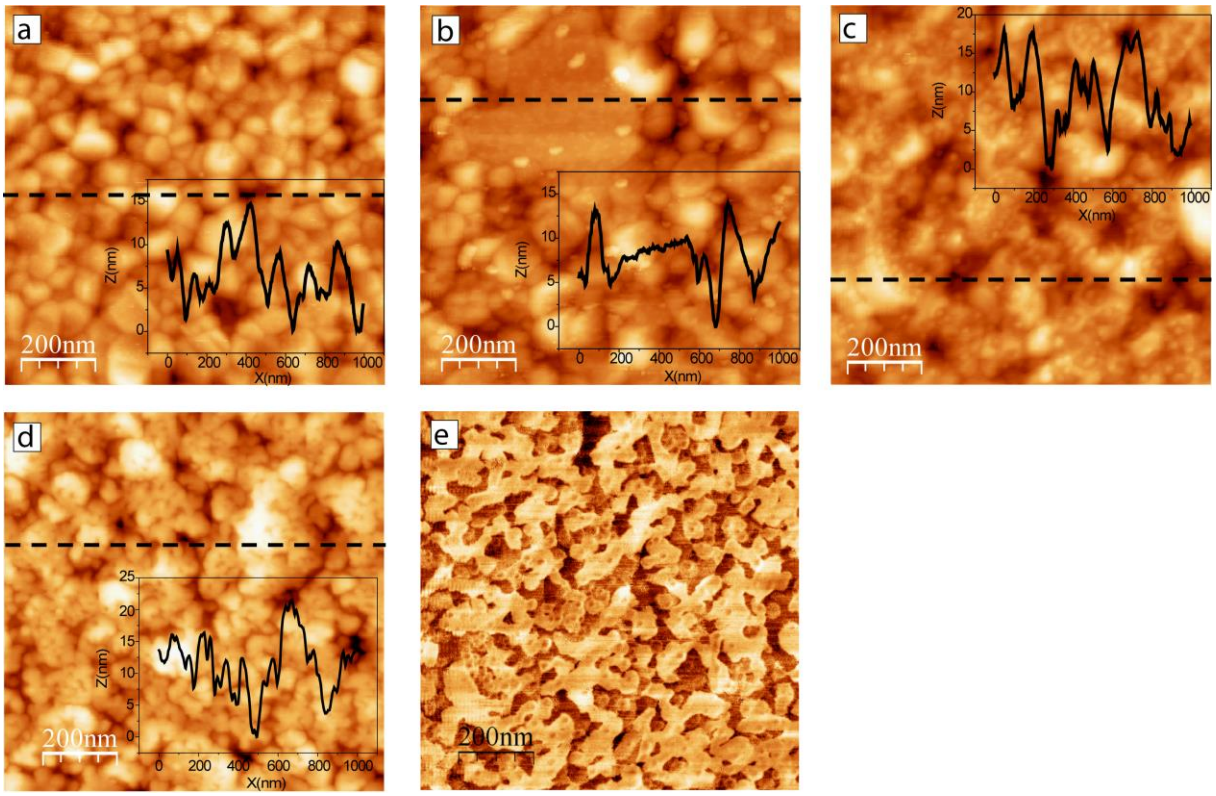

Figure 3: Topographic AFM images including topographic profiles of the bare gold surface (a), the Othiol SAM (b), the Othiol-OGal bilayer (c), and the α-2,6 sialylated surface (d). The sialylated chip was incubated in BSA solution (0.5%). A frequency shift image of the Othiol-OGal bilayer is shown in Figure e. The AFM imaging was conducted in dynamic, non-contact mode.

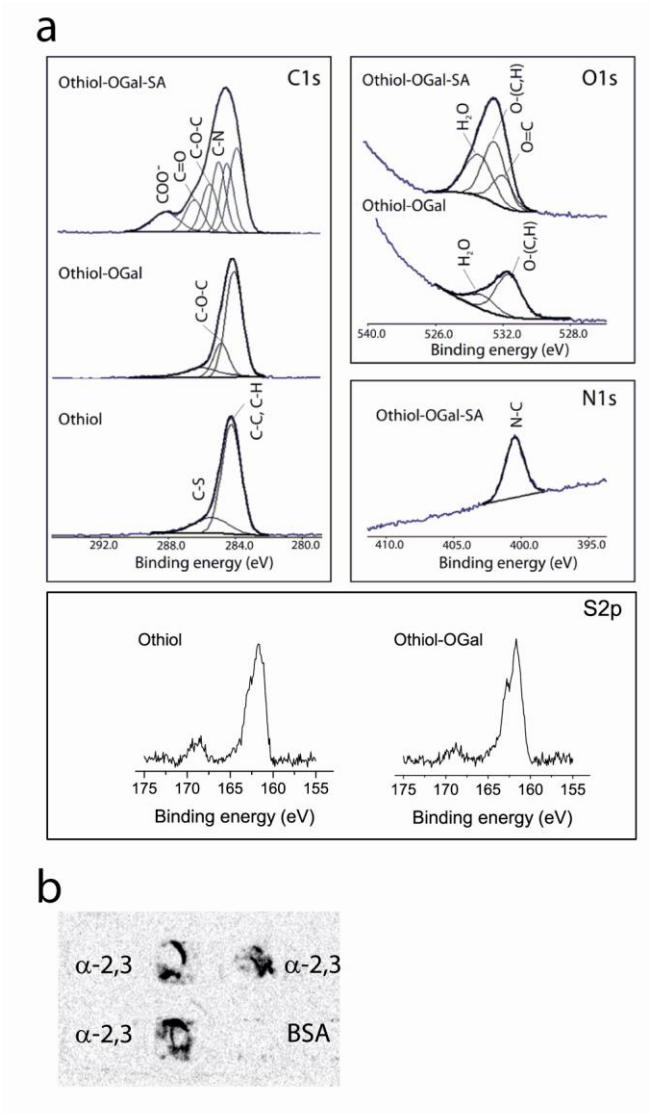

Figure 4. XPS core level spectra of Au supported Othiol, OGal, and SA layers (a). The bands of C1s, O1s, and N1s were deconvoluted with 90 % Gaussian / 10 % Lorentzian peak shapes and the baseline was adjusted with the Tougaard model. Western Blot image (b) of α-2,3 sialylated gold chips after incubation with a H5N9 influenza virus solution (1 μg/ml, 1 h, in triplicate). The dark stains on the chips reveal adsorbed virus and thus, demonstrate the successful α-2,3-sialylation. The control chip was incubated with 1 % BSA.

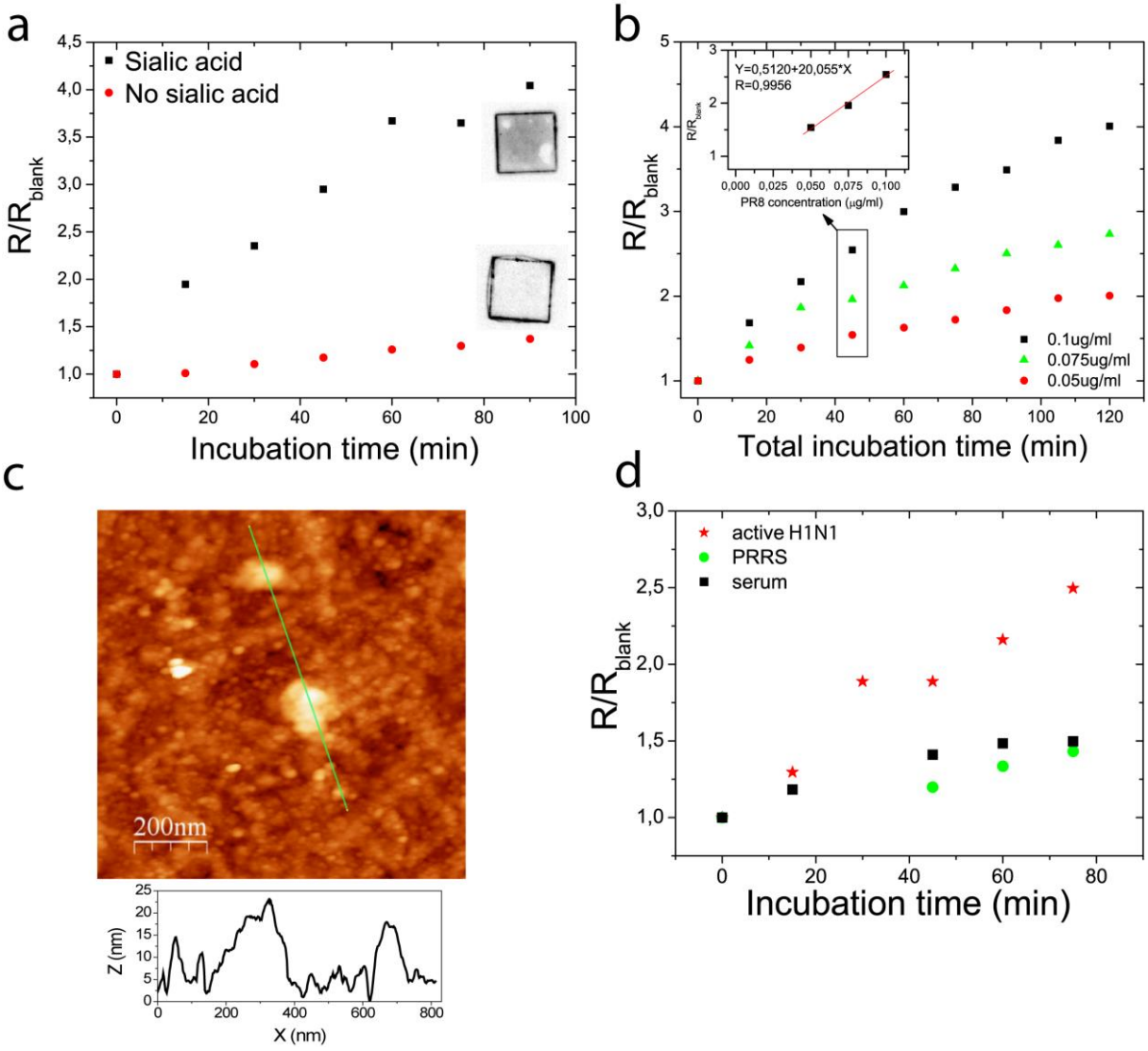

Figure 5. H1N1 adsorption study carried out by incubating sialylated and non-sialylated electrodes in virus solution (0.1 µg ml^{-1}), displaying the WB images of both gold chips after incubation in H1N1 solution (a), and response of the biosensor in solutions containing three different virus concentrations (b). The incubation time refers to the total time during which the electrode surface was successively incubated in the virus solution. The charge-transfer resistance values were calculated by fitting the EIS spectra and the corresponding R/R_{blank} values were extracted from individual blank measurements carried out by incubating the sensors in phosphate buffer saline (PBS). AFM image of an electrode surface that shows two adsorbed virus particles (c) and

biosensor response when incubated in solutions containing serum, Porcine Respiratory and Reproductive Syndrome (PRRS) virus (negative controls) and active H1N1 (positive controls) at 0.01 μg ml^{-1} concentration (d).

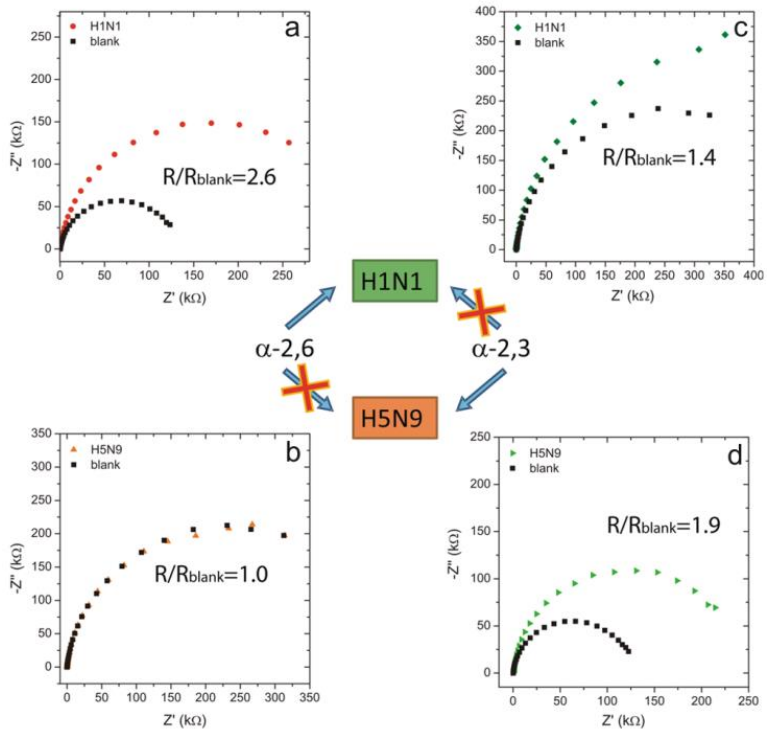

Figure 6. Scheme for selectivity of α-2,6 and α-2,3 sialylated electrodes toward H1N1 and H5N9 influenza viruses together with Nyquist plots of the corresponding EIS assays of the sialylated electrodes after 45 min incubation in solutions of H1N1 and H5N9 virus. Figure a and b refer to α-2,6 sialylated electrodes and Figures c and d refer to α-2,3 sialylated electrodes. The H1N1 and H5H9 virus sample concentrations were 0.1 μg ml^{-1} and 0.75 μg ml^{-1}, respectively. Both samples contained BSA (0.5 %). The signals from virus detection were always related to the corresponding blank signals (R/R_{blank}), which were recorded in PBS solution also containing BSA (0.5 %) in order to correct the absolute magnitude of the recorded Z'/Z" values that can differ between the various electrodes.

Table 1. R_{ct} data obtained from fitting of Nyquist plots to the Randles equivalent circuit model. The spectra were recorded of thiolated gold electrodes that were incubated in 5 mM OGal for 1, 2, or 5 days.

Electrode # / incubation time	Rct [Ω]		
	Othiol	OGal	OGal/Othiol
1/ 1 day	2026	9508	4.69
2 / 2 days	2855	10907	3.82
3 / 5 days	3999	6561	1.64

SYNOPSIS TOC

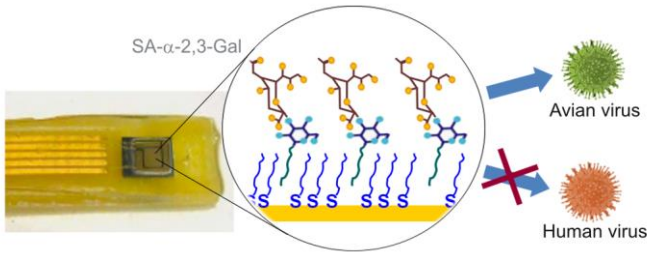

Biomimetic architectures for the impedimetric discrimination of influenza virus phenotypes are tailored by a self-assembly processes on gold substrates. Incorporated sialic acid molecules as sensing entities mimic receptors found on target cells of the influenza A virus. The resulting detector rapidly discriminates between avian vs. human strains of influenza A virus, acting as a reagentless, label-free diagnostic device for influenza phenotyping, which is important in surveillance and prediction of pandemics.